Experimental Study on the Fracture Distribution Characteristics of the Overlying Strata in an Abandoned Gob

Chenlin Wang (wag_cheli@126.com)
Hebei University of Engineering
Xiaodong Zhang
Henan Polytechnic University

Research Article

Keywords: Abandoned gob, Gas, Overlying strata, Fracture, Displacement

Posted Date: November 1st, 2021

DOI: https://doi.org/10.21203/rs.3.rs-992837/v1

Experimental study on the fracture distribution characteristics of the overlying strata in an abandoned gob

Chenlin Wang [1] • Xiaodong Zhang[2,3]

Abstract: A lot of gas resources remain in the abandoned gob. The overlying strata of the abandoned gob are the main places for gas storage and flow. The fracture distribution characteristics of the overlying strata have a significant impact on the gas migration. The mining similarity simulation test device of a plane stress was used to study the deformation and failure characteristics of overlying strata in an abandoned gob. The caved strata of the abandoned gob formed a trapezoidal distribution, and the caving range decreased gradually with an increase in distance from the coal seam. The strata collapsed in the caved zone, whereas the strata collapsed mainly on the bending subsidence in fractured zone. The subsidence curves of caved strata showed a lower concave shape, and the maximum subsidence existed in the middle of the abandoned gob. The caved strata subsidence decreased with an increase in distance from the coal seam. The horizontal fractures were dominant in the fractured zone. The abscission rate of the end mining position was greater than that of the start mining position. Large numbers of vertical fractures existed in the caved zone. The development degree of vertical fractures near the end mining position were larger than that of the start mining position, and the width of the gas-conducting fracture was more than three times that of the start mining position. The development degree, quantity and connectivity of the fracture in the end mining position were better than those in the start mining position.

Keywords: Abandoned gob · Gas · Overlying strata · Fracture · Displacement

✉ Chenlin Wang
wag_cheli@126.com

[1] School of Mining and Geomatics Engineering, Hebei University of Engineering, Handan 056038, China

[2] School of Energy Science and Engineering, Henan Polytechnic University, Jiaozuo 454000, China

[3] Collaborative Innovation Center of Coalbed Methane (Shale Gas) in Central Plains Economic Zone, Henan Polytechnic University, Jiaozuo 454000, China

1 Introduction

China has had abundant coal resources and coal mining operations for more than 100 years. A large area of coal mine gob has formed during long-term coal mining, in which the movement of overlying strata tends to stabilize. This area is termed the abandoned gob after the mining panel closes (Xu, 2011). For the abandoned gob, approximately 50% of the coal remains underground. Gas has not desorbed completely from the residual coal, coal pillar and stress relief coal seam. A certain amount of gas resources remain and accumulate in the abandoned gob (Karacan, 2015; Qin et al., 2015; Meng et al., 2016). The fracture distribution characteristics of the overlying strata in the abandoned gob affect gas storage and flow directly.

During coal seam mining, the overlying gob strata will yield deformation and failure to different degrees. Most researchers have divided the failure characteristics of the overlying strata in the gob into three zones: the caved, fractured and bending zones (Booth and Spande, 1992; Palchik, 2003; Yavuz 2004; Zhang et al. 2019). The surface soil layer has been divided into the soil zone, which is on top of the bending zone, so the overlying strata of the gob were divided into four zones (Peng and Chiang, 1984; Gao 1996). For longwall mining with shallow coal seams, the overlying strata of the gob were divided into two zones: the caved zone and the fractured zone (Wang et al., 2015). For the above three classification methods, the caved zone and the fractured zones appear in the overlying strata of the gob. Large amounts of vertical and horizontal fractures exist in the caved and fractured zone, in which the vertical fractures are several times higher than the mining height, and the horizontal fractures develop within a certain height range (Palchik, 2005; Islam et al., 2009; Sang et al., 2010; Zhang et al., 2011; Majdi et al., 2012; Wei et al., 2016).

The fracture of the overlying strata in the gob is a significant factor that affects gas storage and flow (Karacan, 2007; Palchik 2014; Yang et al., 2014; Fan and Liu, 2017). Vertical fractures are the main channel for gas flow, whereas the horizontal fractures are the main channel for gas storage (Liu, 2011; Li et al., 2014; Qu et al., 2015). After the mining panel was closed, an “O”-shaped circle resulted with mining-induced fractures around the gob. This area is the main channel and space for gas flow (Qian et al., 1998). However, the “O”-shaped circle around the abandoned gob has a widely distributed range, and obvious differences exist in different locations. Therefore, it is necessary to study the fracture distribution characteristics of the overlying strata in the abandoned gob to determine the space of gas flow and storage.

We studied the deformation and failure characteristics of overlying strata in the abandoned gob by a similar simulation experiment. Firstly, we analyzed failure characteristics of overlying strata in the abandoned gob. The collapse law of rock strata was obtained in the caved and fractured zones. Secondly, we analyzed deformation law of the overlying strata in the abandoned

gob. The subsidence curve of overlying strata was obtained. Finally, we analyzed fracture distribution of overlying strata in the abandoned gob. The optimal location of gas flow and storage was determined in the overlying strata of the abandoned gob.

2 Scheme of similar simulation experiment

The research object was panel 3305 in No.5 coal mine, Hebi, Henan Province, China. The mining depth ranged from 502.5 to 552 m. Panel 3305, was 102.8 m wide, 442.05 m long and approximately 527.25 m deep. The average coal seam thickness was 8.26 m with a dipping angle of 8°. The mining method was longwall mining on strike.

2.1 Similarity coefficient

We studied the fracture distribution characteristics of rock strata in the caved and fractured zones of the abandoned gob. According to the similarity criterion, the parameters of the similarity ratio were determined as follows:

$$\text{Geometric similarity} \quad C_L = L_m / L_p = 1:100 \tag{1}$$

$$\text{Poisson ratio similarity} \quad C_\mu = \mu_m / \mu_p = 1 \tag{2}$$

$$\text{Density similarity} \quad C_\rho = \rho_m / \rho_p = 1:1.73 \tag{3}$$

$$\text{Stiffness similarity} \quad C_E = E_m / E_p = C_L \cdot C_\rho = 1:173 \tag{4}$$

$$\text{Stress similarity} \quad C_\sigma = \sigma_m / \sigma_p = C_L \cdot C_\rho = 1:173 \tag{5}$$

$$\text{Time similarity} \quad C_t = t_m / t_p = \sqrt{C_L} = 1:10 \tag{6}$$

where C_L is the geometric similarity; L_m is the model length, cm; L_p is the prototype length, m; C_μ is the Poisson ratio similarity; μ_m is the Poisson ratio of similar materials; μ_p is the Poisson ratio of rock; C_ρ is the density similarity; ρ_m is the density of similar materials, kg/m^3; ρ_p is the rock density, kg/m^3; C_E is the stiffness similarity; E_m is the stiffness of similar materials, N/m; E_p is the rock stiffness, N/m; C_σ is the stress similarity; σ_m is the stress of the overlying strata in the model, kPa; σ_p is the stress of the overlying strata in the prototype, MPa; C_t is the time similarity; t_m is the excavation time of the model, h; and t_p is the panel mining time, h.

2.2 Proportion of similar materials

The dimensions of the model frame were a 2500 mm length, 200 mm width and 1300 mm height in the similar simulation experiment. The experiment materials included mainly sand, gypsum, calcium carbonate and borax (Li, 1988). Sand was the main material with a diameter less than 0.5 mm. Gypsum was used as a cementing material to increase the strength. The calcium carbonate strength was lower and could be used to adjust the strength and deformation properties

of the similar materials. Borax was the retarder and prevented similar materials from coagulating into blocks. The proportion of similar materials was determined by the rock mechanical properties. The proportions and strengths of the similar materials are listed in Table 1. Each rock layer was made according to the proportion of the similar materials. Rock layers were laid from the bottom to the top of the model. After the laying of each rock layer had been completed, an iron block was used to compact the rock layer. The top of the rock layer was sprinkled evenly with mica sheets as the abscission layer.

Table 1 Proportion of similar materials

Lithology	Actual thickness /m	Actual strength /MPa	Simulated thickness /cm	Simulated strength /KPa	Proportion of similar materials	Total weight /kg	Sand/Kg	Calcium carbonate /kg	Gypsum /kg	Borax /g	Water /L
Medium-grained sandstone	7.83	20.25	7.83	117.05	355	70.61	52.96	8.83	8.83	100.87	10.09
Sandy mudstone	14.58	12.36	14.58	71.45	373	127.28	95.46	22.27	9.55	181.83	18.18
Mudstone	2.94	18.69	2.94	108.03	373	25.67	19.25	4.49	1.92	36.67	3.67
Sandy mudstone	12.12	12.36	12.12	71.45	373	105.81	79.36	18.52	7.94	151.15	15.12
Medium-grained sandstone	14.5	20.25	14.5	117.05	355	130.76	98.07	16.35	16.35	186.80	18.68
Sandy mudstone	4.06	12.36	4.06	71.45	373	35.44	26.58	6.20	2.66	50.63	5.06
Medium-grained sandstone	9.87	20.25	9.87	117.05	355	89.01	66.76	11.13	11.13	127.15	12.71
Sandy mudstone	5.78	12.36	5.78	71.45	373	50.46	37.84	8.83	3.78	72.08	7.21
Medium-grained sandstone	5.25	20.25	5.25	117.05	355	47.34	35.51	5.92	5.92	67.64	6.76
Sandy mudstone	7.71	12.36	7.71	71.45	373	67.31	50.48	11.78	5.05	96.15	9.62
二 1 coal seam	8.26	5.63	8.26	32.54	573	38.66	32.21	4.51	1.93	42.95	4.30
Mudstone	1.85	18.69	1.85	108.03	373	16.15	12.11	2.83	1.21	23.07	2.31
Medium-grained sandstone	3.83	20.25	3.83	117.05	355	34.54	25.90	4.32	4.32	49.34	4.93
Sandy mudstone	13.3	12.36	13.3	71.45	373	116.11	87.08	20.32	8.71	165.87	16.59
Fine-sandstone	2.34	23.73	2.34	137.17	473	28.95	23.16	4.05	1.74	32.16	3.22
Mudstone	4.41	18.69	4.41	108.03	373	38.50	28.87	6.74	2.89	55.00	5.50
Limestone	4.23	63.56	4.23	367.40	337	58.37	43.78	4.38	10.22	83.39	8.34
Fine-sandstone	1.61	23.73	1.61	137.17	473	14.52	11.62	2.03	0.87	16.13	1.61
Sandy mudstone	4.66	12.36	4.66	71.45	373	40.68	30.51	7.12	3.05	58.12	5.81

2.3 Layout of displacement monitoring points

To analyze the displacement and deformation law of caved strata in the gob, the displacement monitoring points were laid in the overlying strata of the coal seam. Figure 1 shows the layout of the displacement monitoring points for overlying strata. Seven-layer monitoring points were present and the interval between layers was 10 cm. The interval of adjacent points was 10 cm in each layer. From the bottom to the top of the model, the monitoring line numbers were D1, D2, D3, D4, D5, D6 and D7. The circular monitoring points were noncoding markers, and the square monitoring points were coding markers. The change of displacement monitoring points can reflect caved strata subsidence. A XJTUDP optical close-range photogrammetric system was used to

monitor the caved strata movement. The XJTUDP optical close-range photogrammetric system components are references by Wu et al (2015). After coal seam excavation, the displacement monitoring points were captured by a high-resolution digital camera at different angles and locations when the movement of the caved strata stabilized. The captured photos were read by data analysis software. The software recognized and calculated the three-dimensional coordinates of the target points automatically.

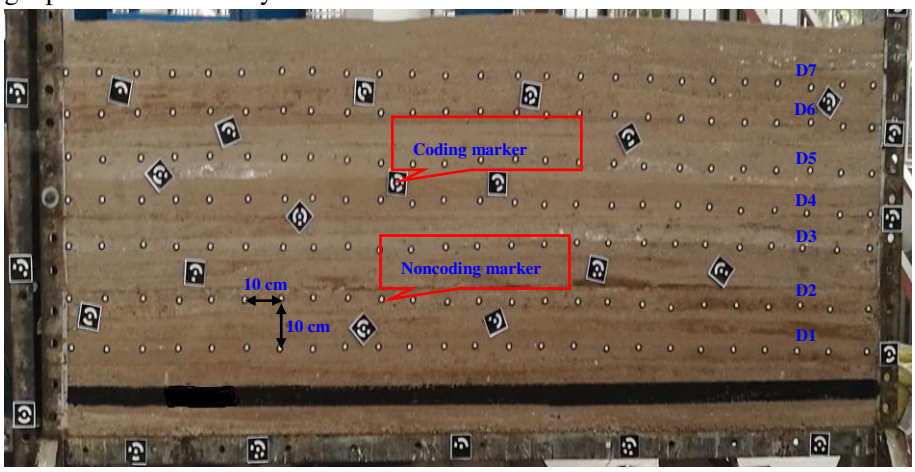

Fig. 1 Layout of the displacement monitoring points

2.4 Model excavation

The protective coal pillar was 30 cm on both sides of the model. The excavation sequence of the model was from left to right, and the excavation step was 10 cm. The excavation time was 30 minutes to ensure that the movement of the caved strata became stable in the gob. A digital camera was used to capture the caving characteristics of the rock strata.

3 Results and analysis

3.1 Caving characteristics of the overlying strata in the gob

The variation characteristics of caved strata in the gob that occur during the mining process are shown in Fig.2. As shown in Fig. 2d, no obvious deformation and failure in the overlying strata of the gob resulted after the coal seam was excavated to 50 cm. When the coal seam was excavated to 60 cm, the immediate roof collapsed as bending subsidence (Fig. 2e). When the coal seam was excavated to 70 cm, the immediate roof collapsed directly (Fig. 2f). When the coal seam was excavated to 90 cm, the D1 line collapsed as bending subsidence. A concave–shaped abscission layer formed between the D1 and D2 lines. The other displacement monitoring lines do not show an apparent collapse (Fig. 2h). When the coal seam was excavated to 100 cm, the caving range of the overlying strata increased visibly and extended to the D3 line. A concave–shaped abscission layer formed between the D3 and D4 lines, and horizontal fractures began to appear at the D4, D5 and D6 lines (Fig. 2i). When the coal seam was excavated to 120 cm, the caving range

of the overlying strata extended to the D5 line. A concave–shaped abscission layer formed between the D5 and D6 lines. A distinct horizontal fracture resulted at the D6 line (Fig. 2k). When the coal seam was excavated to 130 cm, the abscission layer increased between the D5 and D6 lines, and a distinct horizontal fracture existed between the D6 and D7 lines (Fig. 2l). When the coal seam was excavated to 140 cm, the caving range of the overlying strata extended to the D6 line and the abscission layer increased between the D6 and D7 lines (Fig. 2m). When the coal seam was excavated to 160 cm, a concave–shaped abscission layer formed near the D7 line (Fig. 2o). When the coal seam was excavated to 180 cm, the caving range of the overlying strata extended to the top of the model. The amount of abscission layer decreased visibly between the D6 and D7 lines because of gravity action of the caved rock strata (Fig. 2q). When the coal seam was excavated to 190 cm, the caving range of the overlying strata continued to increase, and the caved rock strata formed a trapezoidal shape. The overlying strata collapsed as bending subsidence above the D2 line, whereas the overlying strata collapsed directly below the D2 line. Obvious horizontal fractures existed on both sides of the gob, whereas the abscission layer between the caved strata was compacted in the middle of the gob (Fig. 2r).

Therefore, a concave-shaped abscission layer will appear when an overlying strata collapses. In the middle of the gob, the abscission layer will be compacted as the mining panel continues to advance and the deformation and failure state of the overlying strata have a transition process, which is from the formation of fractures to the compacted state.

(a) The excavation 10 cm

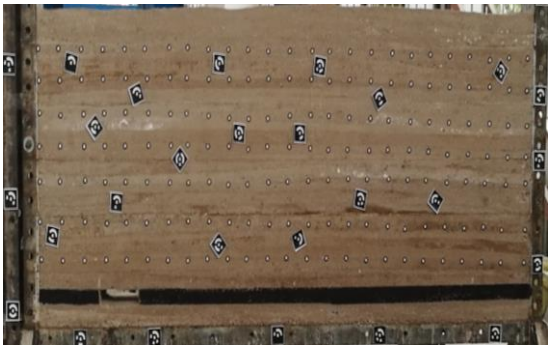

(b) The excavation 20 cm

(c) The excavation 40 cm

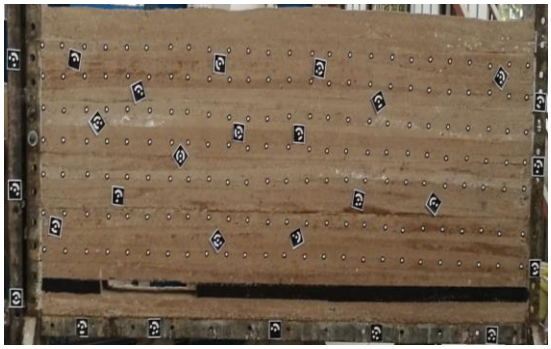

(d) The excavation 50 cm

(e) The excavation 60 cm

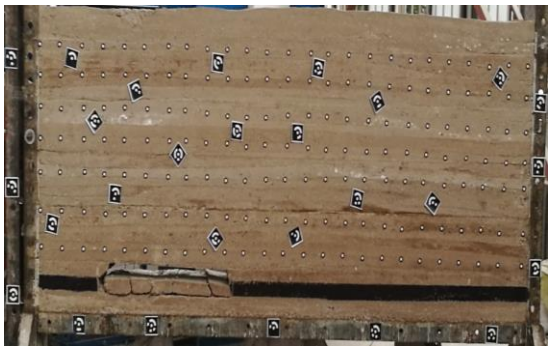

(f) The excavation 70 cm

(g) The excavation 80 cm

(h) The excavation 90 cm

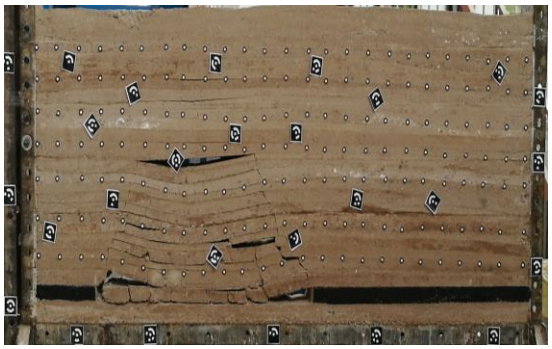

(i) The excavation 100 cm

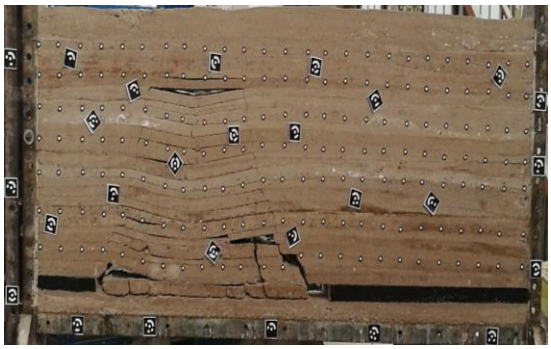

(j) The excavation 110 cm

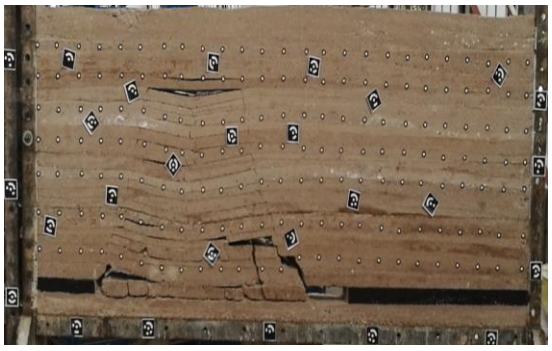

(k) The excavation 120 cm

(l) The excavation 130 cm

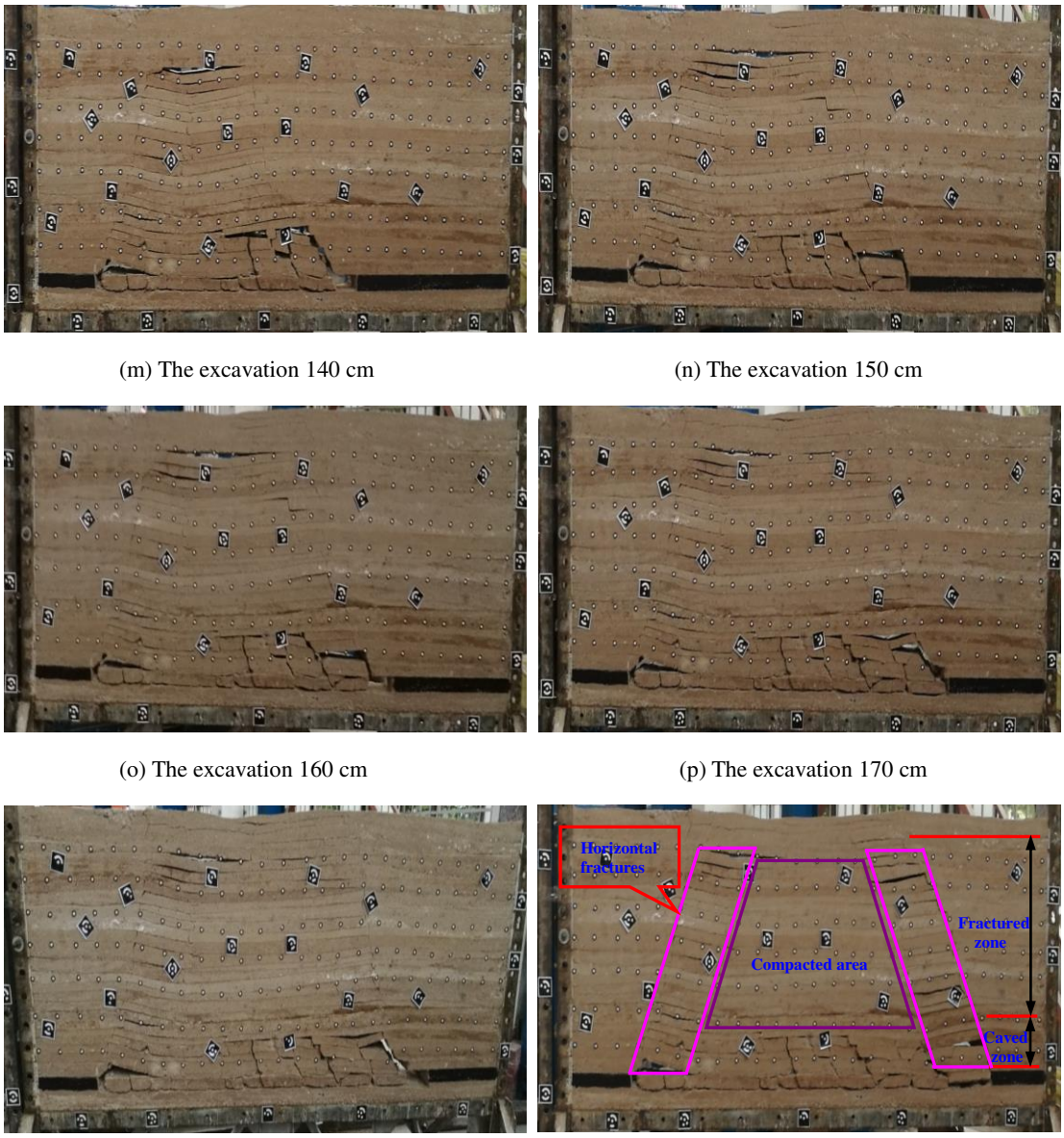

(m) The excavation 140 cm

(n) The excavation 150 cm

(o) The excavation 160 cm

(p) The excavation 170 cm

(q) The excavation 180 cm

(r) The excavation 190 cm

Fig. 2 Caved characteristics of overlying strata during mining

Figure 3 shows the variation characteristics of the caved strata in the gob after 12 h, 24 h and 36 h. It is like the deformation and failure of the caved strata after the nineteenth excavation, which indicates that the deformation and failure of the caved rock strata will not change obviously without a dynamic load disturbance. When the deformation and failure of caved rock strata are stable in the gob, it is termed the abandoned gob. Therefore, the strata collapse mainly on bending subsidence in the fractured zone, whereas the strata collapse in the caved zone. Many horizontal fractures exist on both sides of the abandoned gob, whereas the abscission layer is compressed in the middle of the abandoned gob.

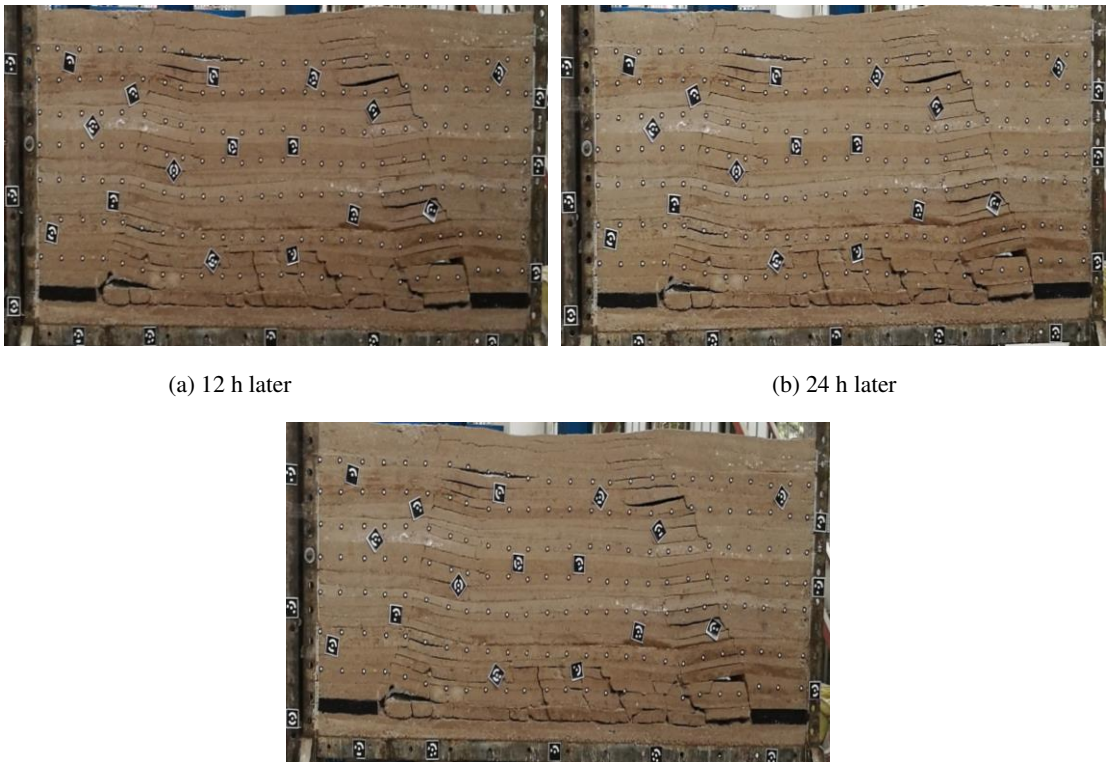

(a) 12 h later (b) 24 h later

(c) 36 h later

Fig. 3 Caving characteristics of overlying strata in the abandoned gob

3.2 Deformation characteristics of the caved strata in the abandoned gob

3.2.1 Subsidence

The subsidence is a variation of caved strata in the vertical direction. It is expressed by the elevation difference between the first and m times the observation of one point in the overlying strata. The formula is as follows:

$$w_n = h_{n0} - h_{nm} \tag{7}$$

where w_n is the subsidence of the n-point in the overlying strata, mm; h_{n0} is the elevation of the n-point at the first observation, mm; and h_{nm} is the elevation of the n-point at the m-times observation, mm.

Figure 4 shows the subsidence curves of caved strata in the abandoned gob. The subsidence curves show a lower concave shape, and the maximum subsidence exists in the middle of the abandoned gob. The subsidence decreases with an increase in distance from the coal seam.

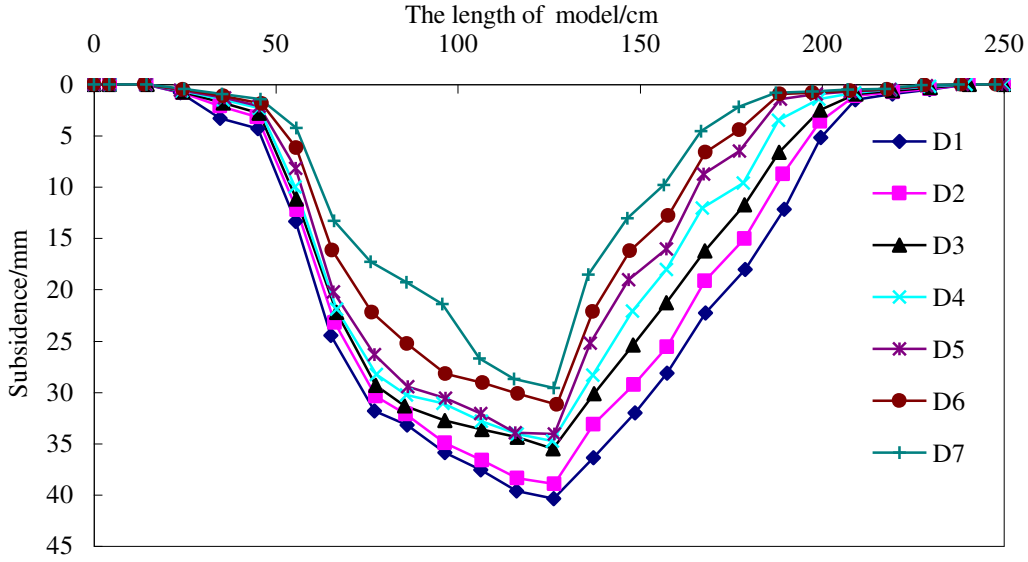

Fig. 4 Subsidence curves of caved strata in abandoned gob

3.2.2 Abscission rate

The abscission rate represents the development height of a fracture in unit thickness strata. The calculation method is the ratio of the subsidence difference between the lower and upper strata to the distance between the upper and lower strata. The formula is as follows:

$$F = \frac{S_d - S_u}{h} \tag{8}$$

where F is the abscission rate, mm·m^{-1}; S_d is the subsidence of the lower strata, mm; S_u is the subsidence of the upper strata, mm; and h is the distance between the upper and lower strata, m.

As shown in Fig. 5, the abscission rate of the right is significantly higher than that on the left side for D1-D2, D2-D3, D3-D4 and D4-D5. That is, the abscission rate near the end mining position is greater than that near the start mining position. The main reason is that the caved strata near the start mining position are affected significantly by periodic weighting of the roof during mining. In contrast, the abscission rate on the left is significantly higher than that on the right for D5-D6 and D6-D7. The main reason is that the upper strata of the model are less affected by the gravity of the caved strata, which experiences a process of gradual expansion.

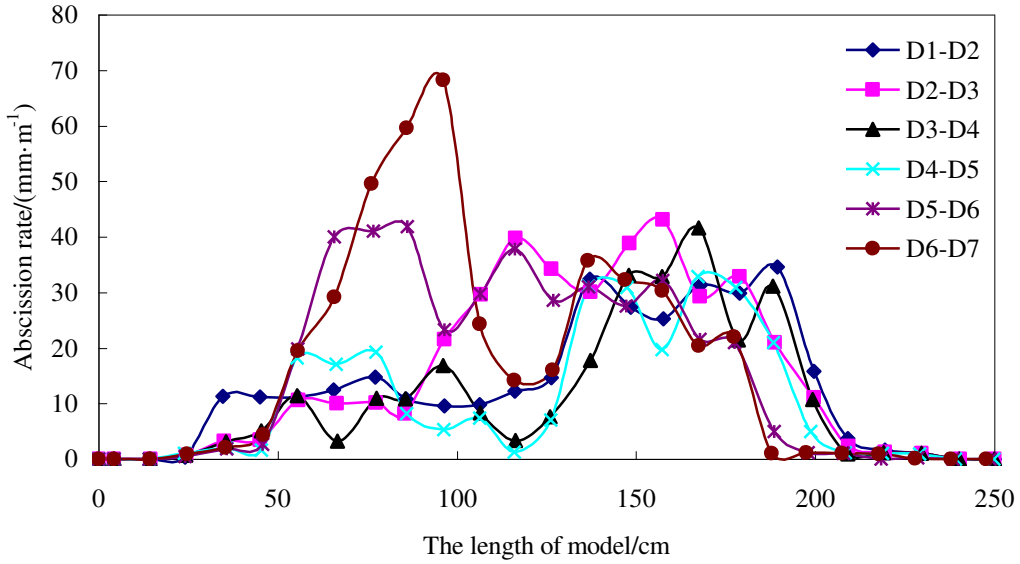

Fig. 5 Variation curves of the abscission rate

3.2.3 Horizontal movement

The horizontal movement is the displacement of the caved strata in a horizontal direction. It is represented by the horizontal distance difference between the m-times and the first observation of one point. The formula is as follows:

$$u_n = l_{nm} - l_{n0} \tag{9}$$

where u_n is the horizontal movement of the n-point, mm; l_{n0} is the horizontal distance between the n-point and the observation line at the first time observation, mm; and l_{nm} is the horizontal distance between the n-point and the observation line at the m times observation, mm.

Figure 6 shows the variation curves of the horizontal movement for the caved strata in the abandoned gob. The caved strata move to the right, and the horizontal movement is positive. The caved strata move to the left, and the horizontal movement is negative. From the start to the end mining position, the horizontal movement shows an increasing–decreasing–increasing trend. The maximum horizontal movement is on both sides of the gob, whereas the minimum horizontal movement is in the middle of the abandoned gob. In the start mining position, the peak points shift gradually to the right with an increase in distance from the coal seam. In the end mining position, the peak valley points shift gradually to the left with an increase in the distance from the coal seam. The main reason is that the range of caved strata decreases with an increase in the distance from the coal seam.

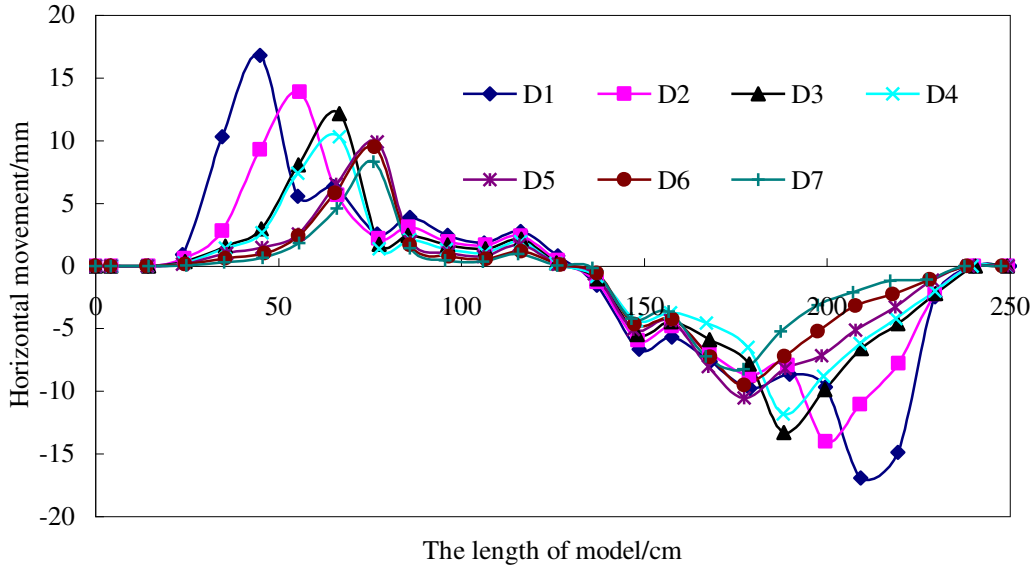

Fig. 6 Variation curves of the horizontal movement

3.2.4 Inclination

The inclination is the ratio of the subsidence difference between the two adjacent points to the horizontal distance. It reflects the slope of the movement for caved strata along one direction. The formula is as follows:

$$i_{m-n} = \frac{w_n - w_m}{l_{n-m}} = \frac{\Delta w_{m-n}}{l_{m-n}} \tag{10}$$

where i_{m-n} is the inclination between m and n points, mm/m; l_{m-n} is the horizontal distance between m and n points, m; and w_n , w_m is the subsidence of m and n points, mm.

Figure 7 shows the variation curves of the inclination for the caved strata in the abandoned gob. The caved strata move to the right, and the inclination is positive. The caved strata move to the left, and the inclination is negative. From the start to the end mining position, the inclination shows an increasing–decreasing–increasing trend. The curve presents an upper convex–lower concave shape. The variation law is the same as the horizontal movement. The maximum inclination is on both sides of the abandoned gob, but the smallest inclination is in the middle of the abandoned gob. With an increase in distance from the coal seam, the inclination decreases gradually and shifts to the middle of the abandoned gob.

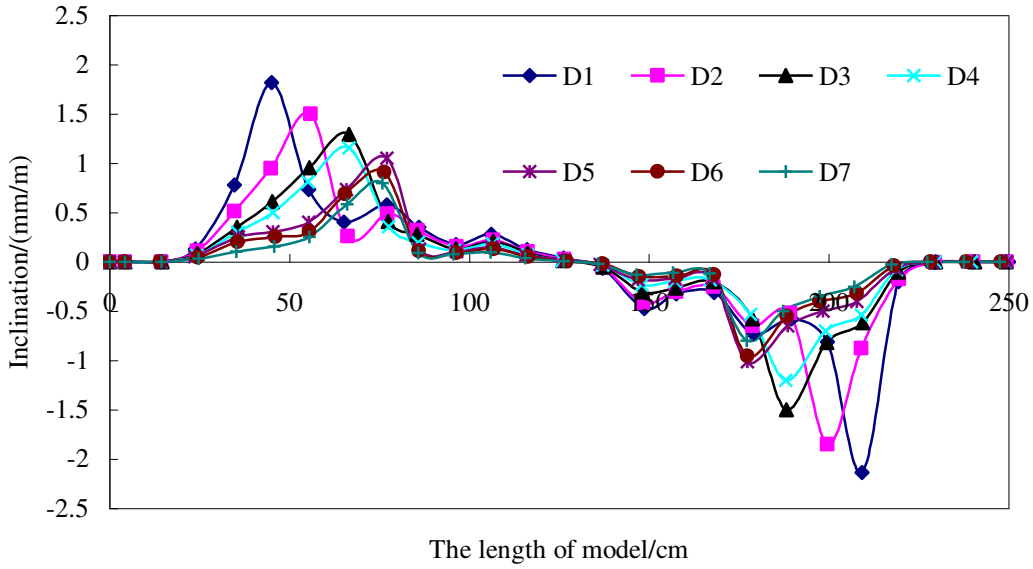

Fig. 7 Variation curves of the inclination

3.2.5 Horizontal deformation

The horizontal deformation is the ratio of the horizontal movement difference between two adjacent points to the horizontal distance. It reflects the stretching or compression of unit length. The formula is as follows:

$$\varepsilon_{m-n} = \frac{u_n - u_m}{l_{m-n}} = \frac{\Delta u_{m-n}}{l_{m-n}} \tag{11}$$

where ε_{m-n} is the horizontal deformation between m and n points, mm/m; u_m and u_n are the horizontal movement of m and n points, respectively, mm; and l_{m-n} is the horizontal distance between m and n points, m.

Figure 8 shows the variation curves of horizontal deformation for the caved strata in the abandoned gob. The caved strata produce tensile deformation, and the horizontal deformation is positive. The caved strata produce compressive deformation, and the horizontal deformation is negative. From the start to the end mining position, the horizontal deformation shows an increasing–decreasing–increasing–decreasing trend. The curve presents an upper convex–lower concave–upper convex shape. The maximum tensile deformation is on both sides of the abandoned gob. The maximum compressive deformation occurs in the middle of the abandoned gob. With an increase in distance from the coal seam, the horizontal deformation decreases gradually, and the peak points move toward the middle of the abandoned gob. The location of the peak valley points remains unchanged in the middle of the abandoned gob.

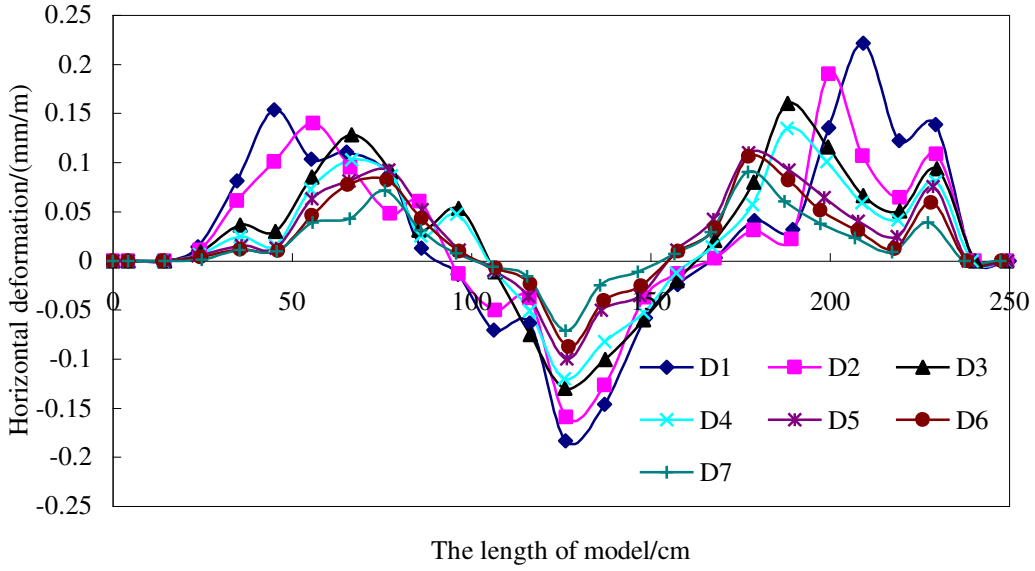

Fig. 8 Variation curves of the horizontal deformation

3.2.6 Curvature

The curvature is the ratio of the inclination difference between two adjacent line segments to the horizontal distance between the middle points of two adjacent line segments. It can reflect the bending degree of the observation section. The formula is as follows:

$$k_{m-n-p} = \frac{i_{n-p} - i_{m-n}}{\frac{1}{2}(l_{m-n} + l_{n-p})} \tag{12}$$

where $k_{m\text{-}n\text{-}p}$ is the mean curvature of line segments m-n and n-p, mm/m^2; $i_{m\text{-}n}$ is the inclination between m and n points, mm/m; $i_{n\text{-}p}$ is the inclination between n and p points, mm/m; $l_{m\text{-}n}$ is the horizontal distance between m and n points, m; and $l_{n\text{-}p}$ is the horizontal distance between n and p points, m.

Figure 9 shows the variation curves of curvature for caved strata in the abandoned gob. The curvature is positive on both sides of the abandoned gob, and negative in the middle of the abandoned gob. From the start to the end mining position, the curvature shows an increasing–decreasing–increasing–decreasing trend. The curve presents an upper convex–lower concave–upper convex shape. The variation curve is consistent with the horizontal deformation. With an increase in distance from the coal seam, the curvature decreases gradually, and the peak points move toward the middle of the abandoned gob. The location of the peak valley points remains unchanged in the middle of the abandoned gob.

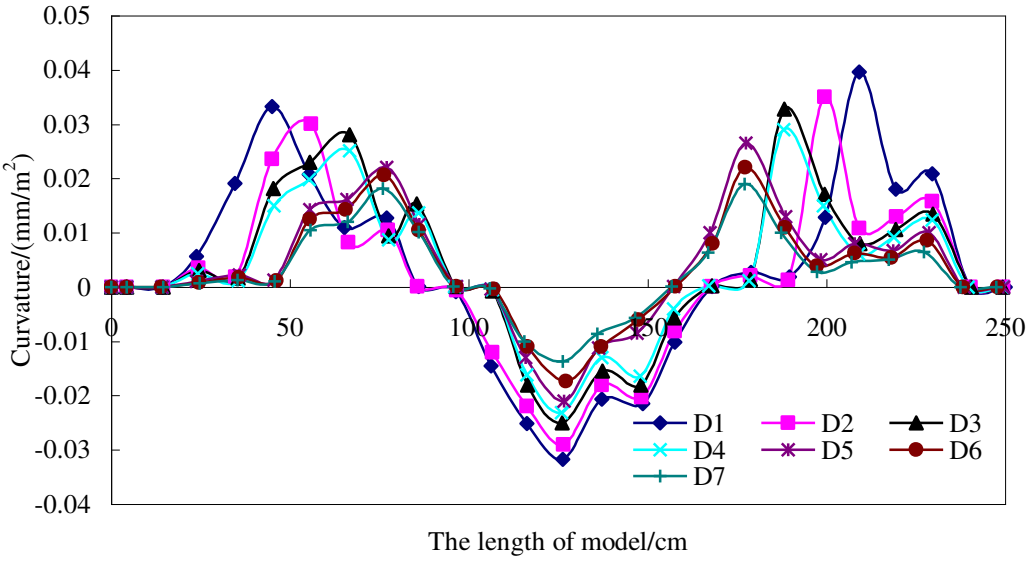

Fig. 9 Variation curves of the curvature

3.3 Fracture distribution characteristics of the caved strata in the abandoned gob

To analyze the fracture distribution characteristics of caved strata in the abandoned gob, Fig.3(c) was processed by binarization. Figure 10 show that the horizontal fractures are dominant on both sides of the abandoned gob. In the bottom of the model, the horizontal abscissions of the end mining position are larger than that of the start mining position according to the calculation results of the abscission rate, and the development degree of vertical fractures near the end mining position is greater than that near the start mining position. The length of the blue line represents the range of gas-conducting fractures in the horizontal direction. The width of gas-conducting fractures is 108.71 cm near the end mining position. The width of the gas-conducting fractures is 35.56 cm near the start mining position. The width of the gas-conducting fractures near the end mining position is more than three times that near the start mining position. Therefore, the development degree, quantity and connectivity of fractures near the end mining position are larger than those near the start mining position. The end mining position is more conducive to gas flow in the abandoned gob.

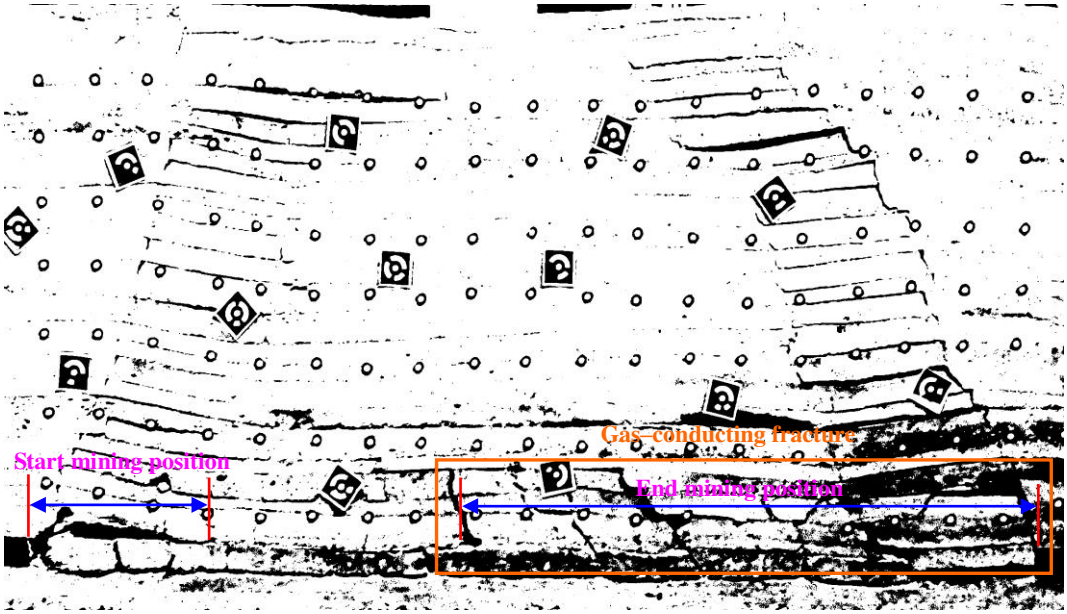

Fig. 10 Fracture distribution characteristics of caved strata in the abandoned gob

4 Conclusions

(1) The caved strata present a trapezoidal distribution, and the caving range decreases gradually with an increase in distance from the coal seam. The strata collapse in the caved zone, whereas the strata collapse mainly on bending subsidence in the fractured zone.

(2) From the start to the end mining position, the subsidence curves of caved strata show a lower concave shape, and the maximum subsidence exists in the middle of the abandoned gob. The subsidence decreases with an increase in distance from the coal seam. The abscission rate near the end mining position is greater than that near the start mining position.

(3) The horizontal fractures are dominant in the fractured zone. Large numbers of vertical fractures in the caved zone. The development degree , quantity and connectivity of fractures near the end mining position is larger than that of the start mining position, and the width of the gas–conducting fracture is more than three times that of the end mining position.

Acknowledgements

The research was provided by the Joint Funds of the National Natural Science Foundation of China (No. U1904126).

References

Booth CJ, Spande ED (1992) Potentiometric and aquifer property changes above subsiding longwall mine panels, illonois basin coalfield. Ground water 30(3): 362-368

Fan L, Liu SM (2017) A conceptual model to characterize and model compaction behavior and permeability evolution of broken rock mass in coal mine gobs. Int J Coal Geol 172: 60-70

Gao YF (1996) “Four-zone” model of rockmass movement and back analysis of dynamic displacement. J Chin Coal Soc 21(1): 51-56 (**in Chinese**).

Islam MR, Hayashi D, Kamruzzaman ABM (2009) Finite element modeling of stress distributions and problems for multi-slice longwall mining in Bangladesh, with special reference to the Barapukuria. Int J Coal Geol 78: 91-109

Karacan CÖ, Esterhuizen GS, Schatzel SJ, Diamond WP (2007) Reservoir simulation-based modeling for characterizing longwall methane emissions and god gas vent hole production. Int J Coal Geol 71(2-3): 225-245

Karacan CÖ (2015) Modeling and analysis of gas capture from sealed sections of abandoned coal mines. Int J Coal Geol 138: 30-41

Li HC (1988) Similar simulation test of underground pressure. China University of Mining and Technology Press, Xuzhou (**in Chinese**)

Li SG, Lin HF, Zhao PX, Xiao P, Pan HY (2014) Dynamic evolution of mining fissure elliptic paraboloid zone and extraction coal and gas. J Chin Coal Soc 39(8): 1455-1462 (**in Chinese**).

Liu YK, Zhou FB, Liu L, Liu C, Hu SY (2011) An experimental and numerical investigation on the deformation of overlying coal seams above double-seam extraction for controlling coal mine methane emission. Int J Coal Geol 87(2): 139-149

Majdi A, Hassani FP, Nasiri MY (2012) Prediction of the height of distressed zone above the mined panel roof in longwall coal mining. Int J Coal Geol 98: 62-72

Meng ZP, Shi CX, Liu SS, Tian YD, Li C (2016) Evaluation model of CBM resources in abandoned coal mine and its application. J Chin Coal Soc 41(3): 537-544 (**in Chinese**).

Palchik V (2003) Formation of fractured zones in overburden due to longwall mining. Environ Geol 44(1): 28-38

Palchik V (2005) Localization of mining-induced horizontal fractures along rock layer interfaces in overburden: field measurements and prediction. Environ Geol 48(1): 68-80

Palchik V (2014) Time-dependent methane emission from vertical prospecting boreholes drilled to abandoned mine working at a shallow depth. Int J Rock Mech Min Sci 72: 1-7

Peng SS, Chiang HS (1984) Longwall Mining. John Wiley & Sons, Inc., New York

Qian MG, Xu JL (1998) Study on the “O-shape” circle distribution characteristics of mining-induced fractures in the overlying strata. J Chin Coal Soc 23(5): 466-469 (**in Chinese**)

Qin W, Xu JL, Hu GZ (2015) Optimization of abandoned gob methane drainage through well placement selection. J Nat Gas Sci Eng 25: 148-158

Qu QD, Xu JL, Wu RL, Qin W, Hu GZ (2015) Three-zone characterisation of coupled strata and gas behaviour in multi-seam mining. Int J Rock Mech Min Sci 78: 91-98

Sang SX, Xu HJ, Fang LC, Li GJ, Huang HZ (2010) Stress relief coadbed methane drainage by surface vertical wells in China. Int J Coal Geol 82: 196-203

Wang FT, Zhang C, Zhang XG, Song Q (2015) Overlying strata movement rules and safety mining technology for the shallow depth seam proximity beneath a room mining goaf. Int J Min Sci Technol 25(1): 139-143

Wei JC, Wu FZ, Yin HY, Guo JB, Xie DL (2016) Formation and height of the interconnected fractures zone after extraction of thick coal seams with overburden in western China. Mine Water Environ 36: 59-66

Wu K, Cheng GL, Zhou DW (2015) Experimental research on dynamic movement in strata overlying mines using similar material modeling. Arab J Geosci 8: 6521-6534

Xu JL (2011) Green mining of coal mine. China University of Mining and Technology Press, Xuzhou (**in Chinese**)

Yang W, Lin BQ, Yan Q, Zhai C (2014) Stress redistribution of longwall mining stope and gas control of multi-layer coal seams. Int J Rock Mech Min Sci 72: 8-15

Yavuz H (2004) An estimation method for cover pressure re-establishment distance and pressure distribution in the goaf of longwall coal mines. Int J Rock Mech Min Sci 41: 193-205

Zhang C, Tu SH, Zhao YX (2019) Compaction characteristics of the caving zone in a longwall goaf: a review. Environ Earth Sci 78: 27

Zhang DS, Fan GW, Ma LQ, Wang XF (2011) Aquifer protection during longwall mining of shallow seams: A case study in the Shendong Coalfield of China. Int J Coal Geol 86: 190-196